Pressure-induced superconductivity in $Ag_xBi_{2-x}Se_3$

Tong He,[1] Xiaofan Yang,[1] Takahiro Terao,[1] Takaki Uchiyama,[1] Teppei Ueno,[1] Kaya Kobayashi,[1] Jun Akimitsu,[1] Takafumi Miyazaki,[2] Takumi Nishioka,[3] Koji Kimura,[3] Kouichi Hayashi,[3,4] Naohisa Happo,[5] Hitoshi Yamaoka,[6] Hirofumi Ishii,[7] Yen-Fa Liao,[7] Hiromi Ota,[8] Hidenori Goto,[1] and Yoshihiro Kubozono[1,*]

[1]*Research Institute for Interdisciplinary Science, Okayama University, Okayama 700-8530, Japan*
[2]*Research Laboratory for Surface Science, Okayama University, Okayama 700-8530, Japan*
[3]*Department of Physical Science and Engineering, Nagoya Institute of Technology, Nagoya 466-8555, Japan*
[4]*Frontier Research Institute for Materials Science, Nagoya Institute of Technology, Nagoya 466-8555, Japan*
[5]*Graduate School of Information Science, Hiroshima City University, Hiroshima 731-3194, Japan*
[6]*RIKEN SPring-8 Center, Hyogo 679-5148, Japan*
[7]*National Synchrotron Radiation Research Center, Hsinchu 30076, Taiwan*
[8]*Advanced Science Research Center, Okayama University, Okayama 700-8530, Japan*

(Received 26 December 2017; published 7 March 2018)

We investigated the pressure dependence of electric transport and crystal structure of Ag-doped Bi_2Se_3. In the sample prepared by Ag doping of Bi_2Se_3, the Bi atom was partially replaced by Ag, i.e., $Ag_{0.05}Bi_{1.95}Se_3$. X-ray diffraction patterns of $Ag_{0.05}Bi_{1.95}Se_3$ measured at 0–30 GPa showed three different structural phases, with rhombohedral, monoclinic, and tetragonal structures forming in turn as pressure increased, and structural phase transitions at 8.8 and 24 GPa. $Ag_{0.05}Bi_{1.95}Se_3$ showed no superconductivity down to 2.0 K at 0 GPa, but under pressure, superconductivity suddenly appeared at 11 GPa. The magnetic field (H) dependence of the superconducting transition temperature T_c was measured at 11 and 20.5 GPa, in order to investigate whether the pressure-induced superconducting phase is explained by either p-wave polar model or s-wave model.

DOI: 10.1103/PhysRevB.97.104503

I. INTRODUCTION

Topological insulators have been extensively studied in the past decade, because of their exciting electronic properties and possible application in electronics [1–15]. A topological insulator is a quantum matter, with a band gap in its bulk structure and gapless states at its surface. These electronic states are completely protected by time-reversal symmetry. Thus, a topological insulator is topologically different from a traditional insulator. The most studied topological insulator is Bi_2Se_3, which has a single Dirac cone [6]. The transport properties of Bi_2Se_3 suggest that its Fermi level does not cross the surface states but a conduction band [9–11], i.e., electrical transport shows metallic behavior in Bi_2Se_3. This is due to a deficiency of Se atoms, providing electrons to shift the Fermi level upward. The angle-resolved photoemission spectrum (ARPES) clearly shows the crossing of the Fermi level to the conduction band of Bi_2Se_3 [10,11]. To lower the Fermi level to match the Dirac point, Ca doping of Bi_2Se_3 was performed, and the resistivity, scanning tunneling spectroscopy, and ARPES measurements showed the complete crossing of the Fermi level to the Dirac point [12,13]. Ca atoms are substituted for Bi atoms to donate holes. Such a Fermi level tuning was also achieved by adjusting the value of x in $Bi_{2-x}Sb_xTe_{3-y}Se_y$ [14,15].

The first discovery of superconductivity in a topological insulator was achieved in Cu-doped Bi_2Se_3, providing a superconducting transition temperature T_c as high as 3.8 K [16]. Here, it should be noted that the Cu atom is not substituted for Bi but is intercalated into the space between two Bi_2Se_3 layers with different orientations, which indicates electron donation to the Bi_2Se_3 layers. Subsequently, Sr doping of Bi_2Se_3, $Sr_{0.065}Bi_2Se_3$, led to superconductivity, with T_c as high as 2.5 K [17]. Here it is reported that the Sr atom is intercalated into the space between layers, indicating electron doping of the Bi_2Se_3 layer. Furthermore, applying pressure to $Sr_{0.065}Bi_2Se_3$ provides superconductivity with a T_c of 8.3 K at 14 GPa [18]. The application of pressure to $Sr_{0.065}Bi_2Se_3$ yielded three different superconducting phases: (1) The T_c rapidly decreased with an increase in pressure up to 1 GPa. (2) A T_c of 4 K emerged at 6 GPa, and slowly decreased up to 12 GPa. (3) A T_c of 8.3 K was suddenly observed at 14 GPa, and it slowly decreased with increasing pressure up to 80 GPa, although the T_c was still above 7 K at 80 GPa. The emergence of three superconducting phases in $Sr_{0.065}Bi_2Se_3$ may be closely related to that of three crystal phases. This superconductivity was assigned to a p-wave coupling. Pressure applied to nondoped Bi_2Se_3 also produced superconductivity, although no superconductivity was observed at ambient pressure [19]. The superconductivity emerged at 12 GPa, and the T_c was 4.4 K. The T_c rapidly increased with increasing pressure up to 17.2 GPa, reaching a maximum T_c of 8.2 K. Further application of pressure up to 24 GPa resulted in a lowering of T_c, which remained constant at 24–32 GPa. This behavior is different from that of Sr-doped Bi_2Se_3. Furthermore, it was found that Nb doping of Bi_2Se_3 produced superconductivity with a T_c as high as 3.2 K [20].

*Corresponding author: kubozono@cc.okayama-u.ac.jp

Here we report the preparation and characterization of Ag-doped Bi_2Se_3, and the pressure dependence of its crystal structure and transport properties. As described later, the Ag-doped Bi_2Se_3 is written as $Ag_{0.05}Bi_{1.95}Se_3$, because the Ag was not intercalated into the Bi_2Se_3 lattice, but substituted for Bi atoms. Therefore, hole doping should be probably achieved for Bi_2Se_3, although not in $Sr_{0.065}Bi_2Se_3$ and $Cu_xBi_2Se_3$, which correspond to electron-doped Bi_2Se_3 [16,17]. Based on this background, we strongly intended to induce superconductivity in hole-doped Bi_2Se_3 (or $Ag_{0.05}Bi_{1.95}Se_3$) by applying pressure. If this could be achieved, it would be the first observation of superconductivity in hole-doped Bi_2Se_3 (i.e., the Fermi level of Bi_2Se_3 is downward tuned).

In this study, the pressure dependence of the crystal structure was determined from pressure-dependent powder x-ray diffraction (XRD) patterns at 0–30 GPa. Moreover, measurement of electric transport at 0–26 GPa showed the emergence of pressure-driven superconductivity at 11 GPa, and the maximum T_c of 7 K was confirmed at 17 GPa. The pressure dependence of T_c was significantly different from that of nondoped Bi_2Se_3 [19], and was similar to that of $Sr_{0.065}Bi_2Se_3$ [18]. The superconductivity was fully investigated from the magnetic field (H) dependence of T_c at 11 and 20.5 GPa.

II. EXPERIMENTAL PROCEDURE AND CHARACTERIZATION

Crystals of Ag-doped Bi_2Se_3, $Ag_{0.05}Bi_2Se_3$, were grown by a conventional melt-growth method using stoichiometric amounts of Ag, Bi, and Se powders. The detailed process was as follows: the powders were sealed in a quartz tube which was heated at 800 °C for 12 h, then slowly cooled down to 650 °C at the rate of 30 °C/h, and then quenched with ice water. The obtained crystals showed a clear basal plane structure. An optical image of a crystal-like $Ag_{0.05}Bi_2Se_3$ lump is shown in Fig. 1(a).

The energy-dispersive x-ray spectroscopy (EDX) spectrum of the $Ag_{0.05}Bi_2Se_3$ lump (not shown) was recorded with an EDX spectrometer equipped with a scanning electron microscope (KEYENCE VE-9800-EDAX Genesis XM2). The EDX spectra were measured for five different positions of the $Ag_{0.05}Bi_2Se_3$ lump at room temperature. From the EDX spectra, the chemical composition of the $Ag_{0.05}Bi_2Se_3$ sample was determined to be $Ag_{0.061(7)}Bi_2Se_{3.54(8)}$, in which the quantity of Bi was adjusted to 2, showing the presence of Ag in this crystal. Since the deviation of stoichiometry for Se is a little large, this problem is discussed later.

The crystal structure was determined by single-crystal XRD measurement of the $Ag_{0.05}Bi_2Se_3$ crystal, which was obtained by cutting off a small piece (~100-μm scale) of the lump of $Ag_{0.05}Bi_2Se_3$, and using a Rigaku Saturn 724 diffractometer equipped with a Mo Kα source (wavelength $\lambda = 0.71073$ Å); the measurement was performed at 100 K. The crystal structure was rhombohedral (space group: $R\bar{3}m$) which is consistent with that of Bi_2Se_3 [21]. The lattice constants a and c were determined to be 4.146(6) and 28.66(4) Å, respectively, which are close to those of Bi_2Se_3 (4.18 and 28.7 Å) [21]. Admittedly, the c values are not so expanded in $Cu_xBi_2Se_3$ ($c = 28.736(1)$ Å [16]) and $Sr_xBi_2Se_3$ ($c = 28.598$ Å [17]) in which Cu and Sr are intercalated into the space between Bi_2Se_3 layers. The c value [=28.66(4) Å] of Ag-doped Bi_2Se_3 is an intermediate value between the c values of $Cu_xBi_2Se_3$ and $Sr_xBi_2Se_3$. In any case, it is difficult to identify whether Ag is intercalated or substituted for Bi from the lattice constant c. A refined view of the crystal structure shows that no Ag atoms appear in any location other than the 6c and 3a sites, indicating that the Ag atom may not be intercalated, i.e., the chemical composition can be expressed as $Ag_{0.05}Bi_{1.95}Se_3$. The structural information is fully described elsewhere [22].

Finally, a multiple-energy x-ray fluorescence hologram around a Ag atom in the $Ag_{0.05}Bi_2Se_3$ was measured at BL13XU of SPring-8. Ag Kα fluorescent x rays (22.16 keV) were collected using an avalanche photodiode detector via a cylindrical graphite crystal energy analyzer, at 11 different incident x-ray energies from 26.0 to 31.0 keV in steps of 0.5 keV. Experimental details are given elsewhere [23]. Figure 1(b) shows a real image of the local structure around a Ag atom, reconstructed from an x-ray fluorescence hologram of the $Ag_{0.05}Bi_2Se_3$ crystal using the Barton multiple-energy reconstruction algorithm [24]. This image suggests that the Ag atom is surrounded by six Bi atoms in a hexagonal arrangement, indicating that Ag is partially substituted for Bi. The chemical composition can be expressed as $Ag_{0.05}Bi_{1.95}Se_3$. It would be written as $Ag_{0.059(7)}Bi_{1.941}Se_{3.44(8)}$ if using the EDX's result. The stoichiometry of Se, 3.44(8), deviates from the nominal value of Se, 3.0. We further evaluated the stoichiometry from the EDX spectra measured for six $Ag_{0.05}Bi_2Se_3$ single crystals prepared in the same experimental conditions, including the above single crystal. The averaged stoichiometry was expressed as $Ag_{0.09(2)}Bi_{1.91}Se_{3.1(6)}$ (=$Ag_{0.09(2)}Bi_2Se_{3.2(6)}$). The averaged value of Se's stoichiometry evaluated from six single crystals is closer to 3.0 than the value evaluated for one selected single crystal described above. Actually, the estimated standard deviation is a little large, and it is unclear whether the Se is deficient or excessive in comparison with the nominal value 3.0. Thus, the stoichiometry of Se is a little scattered around 3.0 depending on the used crystals.

Therefore, we employ the EDX data only to confirm that Ag is contained in the crystal. Consequently, the sample's chemical formula is written as $Ag_{0.05}Bi_{1.95}Se_3$ throughout this paper by considering the substitution of Bi with Ag, and the scattering of stoichiometry of Se around 3.0 depending on crystals. The partial substitution of Bi with Ag indicates a possible hole doping in $Ag_xBi_{2-x}Se_3$, i.e., the Fermi level of Bi_2Se_3 is downward tuned. The drastic change of transport property in $Ag_xBi_{2-x}Se_3$ with respect to that in Bi_2Se_3 also suggests a hole doping [22]. Namely, the transport property of $Ag_xBi_{2-x}Se_3$ showed an insulating behavior at high temperature range, in contrast to a metallic one of Bi_2Se_3, which was reasonably explained by a downward shift of the Fermi level caused by hole doping.

Powder XRD patterns of the $Ag_{0.05}Bi_{1.95}Se_3$ sample were measured under pressure at 297 K, using synchrotron radiation at BL12B2 of SPring-8; the wavelength λ of the x-ray beam was 0.6889 Å. The powder sample obtained by grinding the $Ag_{0.05}Bi_{1.95}Se_3$ lump was used for the powder XRD measurement. A diamond-anvil cell (DAC) was used for the high-pressure XRD measurement, with the powder sample

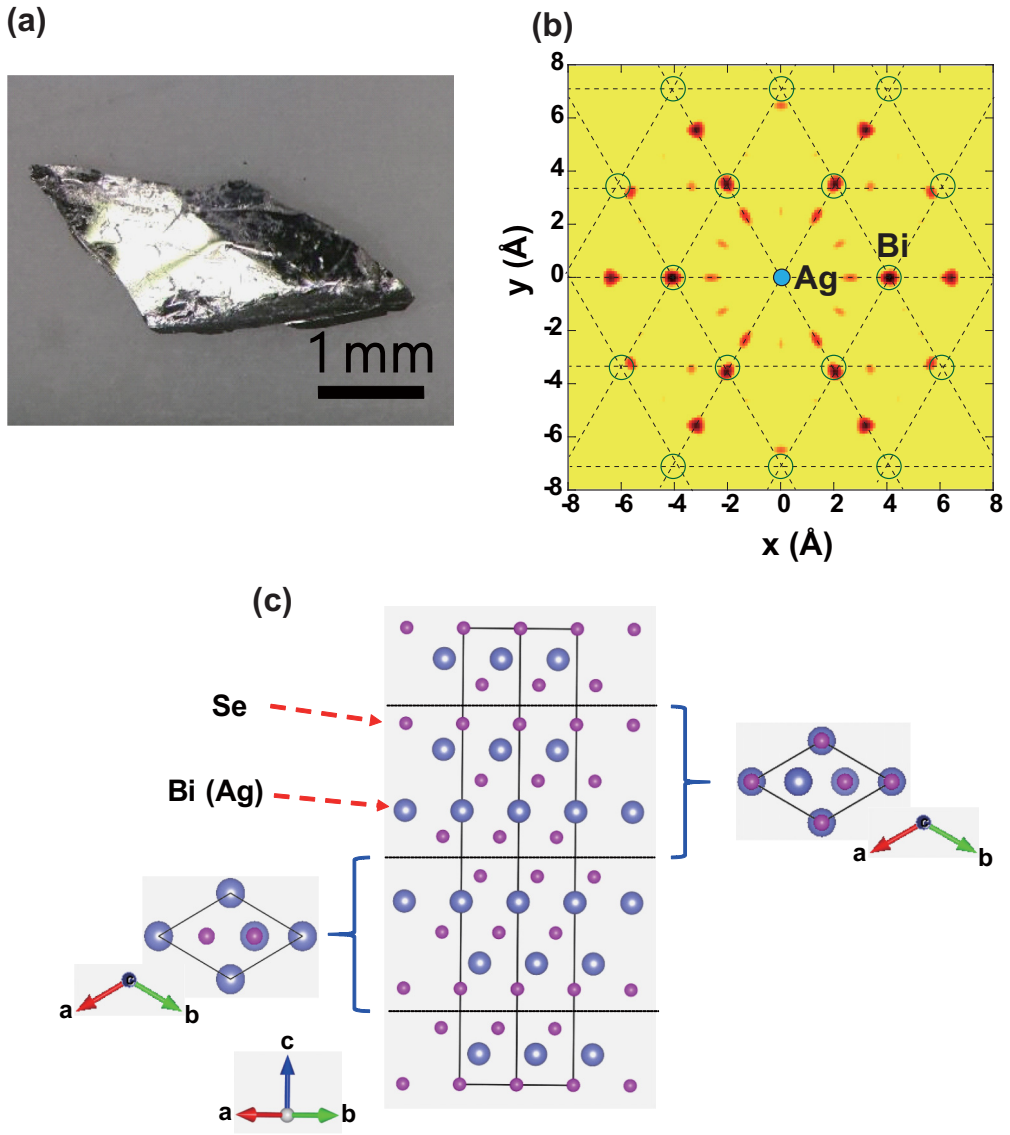

FIG. 1. (a) Optical image of a crystal-like lump of $Ag_{0.05}Bi_{1.95}Se_3$. (b) Real-space image of the local structure around a Ag atom in $Ag_{0.05}Bi_{1.95}Se_3$ reconstructed from the x-ray fluorescence hologram. The Ag atom is at the origin of this image. (c) Crystal structure of $Ag_{0.05}Bi_{1.95}Se_3$, determined from single-crystal x-ray diffraction analysis at 0 GPa.

loaded into the hole of an SUS plate. Daphne 7373 was used as the pressure medium for XRD measurement under high pressure. The pressure was determined by monitoring ruby fluorescence.

The dc magnetic susceptibility (M/H) of the small lumps (1-mm scale) of $Ag_{0.05}Bi_{1.95}Se_3$ was recorded by a superconducting quantum interference device magnetometer (Quantum Design MPMS2) at ambient pressure (0 GPa). M and H refer to magnetization and applied magnetic field, respectively. The temperature dependence of the resistance (R) of a small lump (200-μm scale) of $Ag_{0.05}Bi_{1.95}Se_3$ was measured in four-terminal measurement mode under pressure. The small $Ag_{0.05}Bi_{1.95}Se_3$ lump was introduced into the DAC in air because this sample is not air-sensitive. The sample was loaded directly on a Kapton sheet/epoxy resin/rhenium in the DAC; six Cu electrodes were attached to the Kapton sheet, and this cell was used for measuring the R of sample. NaCl was used as the pressure medium for the R measurement under high pressure. The applied pressure was determined by monitoring ruby fluorescence.

The R of the sample was measured in standard four-terminal measurement mode using an Oxford superconducting magnet system. The temperature was precisely regulated using an Oxford Instruments MercuryiTC. The H was controlled using Oxford Instruments MercuryiPS. Electric current (I) was supplied by a Keithley 220 programmable current source, and the exact value of I was monitored by an Advantest R-8240 digital electrometer. The voltage (V) was measured by an Agilent 34420 digital nanovoltmeter.

III. RESULTS AND DISCUSSION

Figure 1(c) shows the crystal structure of $Ag_{0.05}Bi_{1.95}Se_3$ as determined from single-crystal x-ray diffraction analysis at

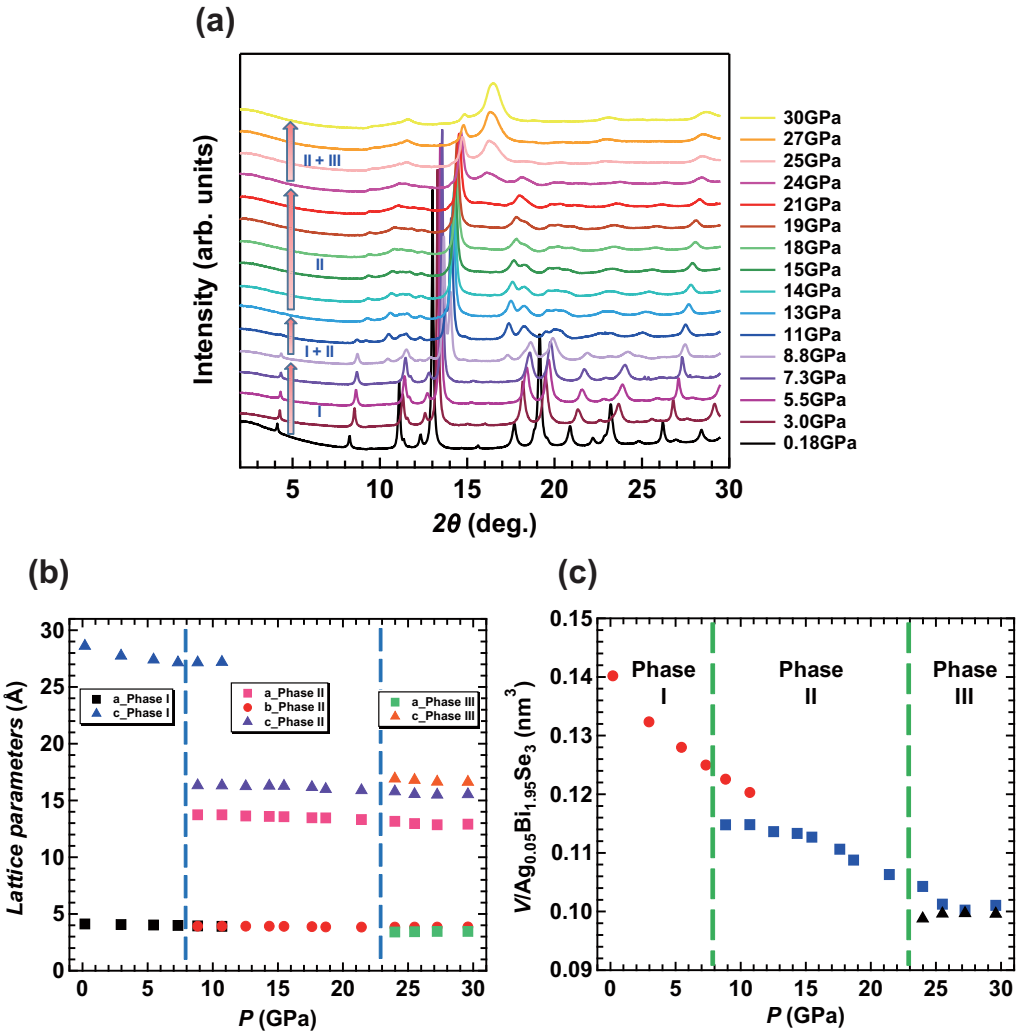

FIG. 2. (a) Powder XRD patterns of $Ag_{0.05}Bi_{1.95}Se_3$ at 0–30 GPa. Pressure dependence of (b) lattice constants of $Ag_{0.05}Bi_{1.95}Se_3$ and (c) volume per one $Ag_{0.05}Bi_{1.95}Se_3$.

0 GPa. The crystal lattice consisted of two asymmetry units ($2 \times Bi_2Se_3$), showing two-dimensional crystal structure. Figure 2(a) shows the XRD patterns at 0–30 GPa, which indicate clear structural phase transitions at 8.8 and 24 GPa. By analogy with the structural transitions of $Sr_{0.065}Bi_2Se_3$ [18], the first structure below 8.8 GPa was assigned to a rhombohedral structure [space group: $R\bar{3}m$ (No. 166)], while the second structure at 8.8 GPa $\leqslant p \leqslant$ 21 GPa and the third structure above 21 GPa were assigned, respectively, to monoclinic [space group: $C2/m$ (No. 12)] and tetragonal structures [space group: $I4/mmm$ (No. 139)]. The pressures driving structural transitions were almost the same as those, 8.1 and 25 GPa, for $Sr_{0.065}Bi_2Se_3$. The first, second, and third structures are called phase I, phase II, and phase III, respectively. As seen from Fig. 2(a), small XRD peaks due to phase I are still found in addition to those of phase II at $p = 8.8$–11 GPa, but the peaks due to phase I substantially disappear above 11 GPa. On the other hand, the peaks due to phase II are observed together with those due to phase III at $p \geqslant 24$ GPa, although the intensity of the phase II peaks diminishes with pressure; the volume fractions of phase II and phase III were not determined in the pressure range, but the phase II drastically decreased when increasing pressure above 24 GPa. A similar pattern of behavior is also found in $Sr_{0.065}Bi_2Se_3$ [18], i.e., the phase transition is not very sharp as pressure changes, but a bit broad.

Le Bail fitting was achieved for the XRD patterns of $Ag_{0.05}Bi_{1.95}Se_3$ by assuming the above crystal structures at each pressure. The lattice constants were determined by Le Bail fitting as follows. Lattice constants a and c at 0.18 GPa ($R\bar{3}m$) were 4.1420(1) and 28.612(3) Å, respectively. Constants a, b, and c, and β at 13 GPa ($C2/m$) were 13.637(1), 3.9252(6), and 16.251(3) Å, and 148.874(4)°, respectively. Furthermore, a and c at 30 GPa ($I4/mmm$) were 3.4611(4) and 16.628(2) Å, respectively. Figures 2(b) and 2(c) show the pressure dependence of lattice constants and volume per one $Ag_{0.05}Bi_{1.95}Se_3$. As seen in Fig. 2(c), a discontinuous change of volume is observed at 8.8 and 24 GPa, indicating the first-order phase transition. To be exact, as seen from Fig. 2(c), the transition at 24 GPa may not be so sharp, i.e., the V of phase II approaches that of phase III at around 26 GPa. Thus, $Ag_{0.05}Bi_{1.95}Se_3$ shows pressure-induced multiple structural phase transitions as pressure varies from 0 to 30 GPa.

The M/H-T plot of $Ag_{0.05}Bi_{1.95}Se_3$ at 0 GPa (not shown) did not show any superconducting transition down to 2.5 K,

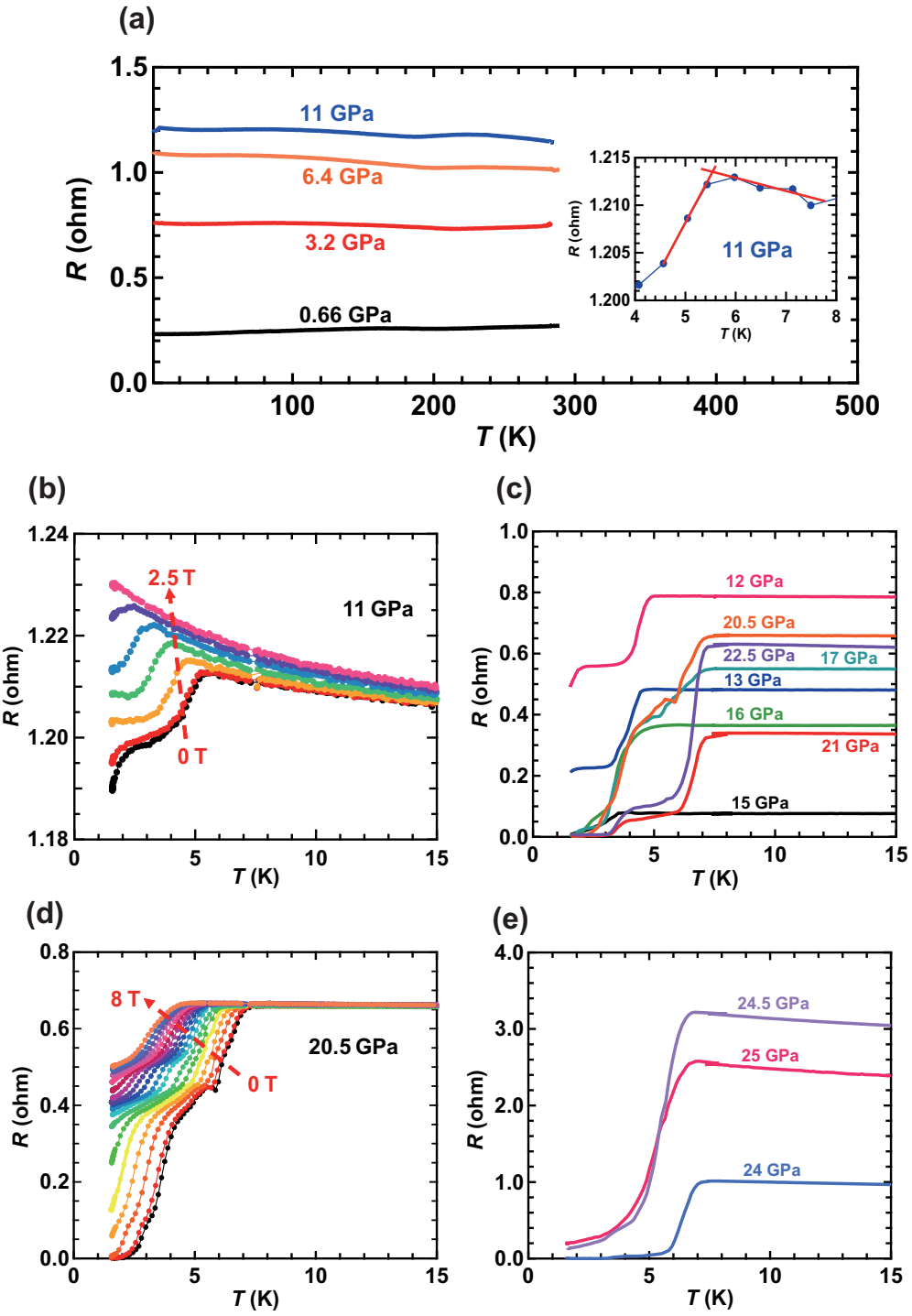

FIG. 3. (a) R-T plots of $Ag_{0.05}Bi_{1.95}Se_3$ at 0–11 GPa. (b) R-T plots of $Ag_{0.05}Bi_{1.95}Se_3$ at different H's at 11-GPa pressure. (c) R-T plots of $Ag_{0.05}Bi_{1.95}Se_3$ at 12–22.5 GPa. (d) R-T plots of $Ag_{0.05}Bi_{1.95}Se_3$ at different H's at 20.5-GPa pressure. (e) R-T plots of $Ag_{0.05}Bi_{1.95}Se_3$ at 24–25 GPa; the R-T plot at 26 GPa is not shown because only the R-T plot was measured in two-terminal measurement mode and the R values were very high, although the superconducting transition was clearly found.

implying that $Ag_{0.05}Bi_{1.95}Se_3$ is not a superconductor at 0 GPa. The R-T plots of $Ag_{0.05}Bi_{1.95}Se_3$ at 0–6.4 GPa show no drop in R even at low temperature [Fig. 3(a)], indicating no superconducting transition. On the other hand, a slight drop in R was observed at 11 GPa [inset of Fig. 3(a)], indicating the emergence of a superconducting transition. The T_c was 5.5 K at 11 GPa. To confirm that the drop was due to a superconducting transition, the H dependence of the R-T plot was investigated at 11 GPa from 0.0 to 2.5 T. It was seen that the R drop was suppressed with H, and the T_c decreased gradually [Fig. 3(b)].

With increasing pressure, the R drop became clearer, as seen from Figs. 3(c)–3(e). The minimum R below T_c approached

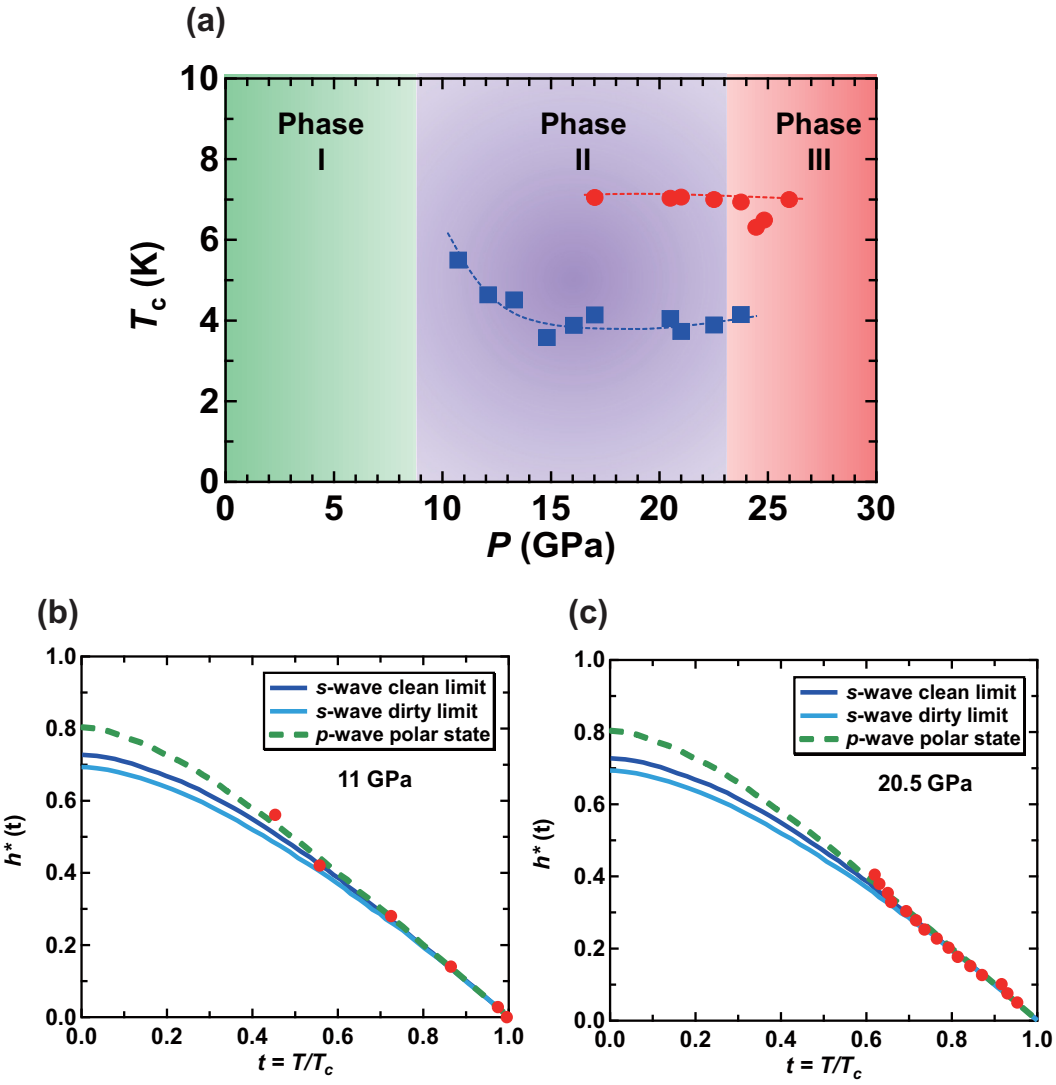

FIG. 4. (a) Pressure dependence of T_c in $Ag_{0.05}Bi_{1.95}Se_3$ (T_c–p phase diagram). $h^*(t)$–t plots of the superconducting phases in $Ag_{0.05}Bi_{1.95}Se_3$ at (b) 11 and (c) 20.5 GPa. The solid and dashed lines refer to the theoretical $h^*(t)$–t curves (s-wave and p-wave model), respectively [see (b) and (c)].

zero. Furthermore, two step R drops were observed in the pressure range of 17 to 24 GPa, and only a single drop was found above 24 GPa [see Fig. 3(e)]. The H dependence of the R-T plot was investigated at 20.5 GPa [Fig. 3(d)], and shows that the R drop is suppressed with H, and the T_c decreases gradually. Thus, it has been confirmed that the R drop can be confidently assigned to a superconducting transition, a result that provides an observation of superconductivity in hole-doped Bi_2Se_3. The analyses of R-T plots did not lead to consideration of the small drop of R observed below 3.0 K, because of the possibility of a superconducting transition of rhenium showing the $T_c \leqslant 3.3$ K at 0–20 GPa, which was used inside of DAC, although no contact between electrodes and rhenium was confirmed at any pressure.

The absolute R above T_c (normal state) increased with increasing pressure up to 11 GPa, but it showed a complex change against pressure above 11 GPa as follows: (1) The R value in the normal state suddenly decreased at 15 GPa, and gradually increased up to 20.5 GPa. (2) The R value suddenly decreased at 21 GPa, and then it rapidly increased against pressure above 21 GPa. Aside from the behavior of the R value at 21 GPa, the R value in the normal state increases with increasing pressure above 11 GPa. At the present stage, such a complex change cannot be well explained, i.e., we cannot say clearly whether it is owing to an intrinsic behavior or a variation of experimental condition such as contact. Therefore, in this study we will comment on only a superconducting transition shown in R-T plots (Fig. 3), because it can be unambiguously and exactly explored.

Figure 4(a) shows the pressure dependence of the T_c of $Ag_{0.05}Bi_{1.95}Se_3$ which was determined from the R-T plots shown in Figs. 3(a), 3(c), and 3(e). As seen in Fig. 4(a), superconductivity emerged in phase II, and no superconductivity is observed in phase I. Two superconducting phases (high-T_c and low-T_c phases) are observed at 17–24 GPa which is still in phase II categorized from XRD patterns. The high-T_c phase

shows $T_c \sim 7$ K, while the low-T_c phase shows $3.6\,\mathrm{K} \leqslant T_c \leqslant 5.5$ K. The low-T_c phase completely disappeared in phase III. This behavior is similar to that of $Sr_{0.065}Bi_2Se_3$, providing two superconducting phases in phase II [18]. However, two superconducting phases did not coexist in $Sr_{0.065}Bi_2Se_3$, unlike in $Ag_{0.05}Bi_{1.95}Se_3$.

Here, we suggest the scenario that a slow variation from phase II relating to low-T_c superconductivity to phase III relating to high-T_c superconductivity takes place before the structural transition of phase II to phase III is observed above 23 GPa. Namely, phase III may extend gradually from 17 GPa, suggesting that phase III is filamentary formed above 17 GPa before the formation of bulk phase III above 23 GPa. Although phase II is still observed above 23 GPa in the XRD pattern, a drastic decrease in phase II makes it difficult to detect the low-T_c phase above 23 GPa.

The behavior of T_c with pressure in $Ag_{0.05}Bi_{1.95}Se_3$ is significantly different from that in Bi_2Se_3 where only a single superconducting phase was observed above 10 GPa [19]. Precisely stated, the T_c of Bi_2Se_3 increases continuously up to 17.2 GPa, then decreases up to 20 GPa, and finally becomes constant above 24 GPa. Thus, the pressure dependence of T_c in $Ag_{0.05}Bi_{1.95}Se_3$ does not show similarity to Bi_2Se_3 but to $Sr_{0.065}Bi_2Se_3$. Here, we must stress that the pressure-driven superconductivity in $Ag_{0.05}Bi_{1.95}Se_3$ relates closely to the structural phase transitions. Therefore, the electronic properties in phase II and phase III, where different superconducting phases emerge, must be clarified from the pressure-dependent Hall-effect and x-ray emission spectroscopy as well as theoretical calculation; we do not have any calculation supporting that the monoclinic and tetragonal phases of Ag-doped Bi_2Se_3 are topological materials. These works are now in progress.

Finally, we must consider whether this superconductivity should be categorized as "unconventional superconductivity" (or "topological superconductivity"). The previous study of the temperature dependence of the upper critical field, H_{c2}, of $Sr_{0.065}Bi_2Se_3$ showed that the superconductivity may originate in spin-triplet p-wave coupling [18]. In this study, the values of the reduced critical field, $h^*(T) = [\frac{H_{c2}(T)}{T_c}]/[-\frac{dH_{c2}(T)}{dT}]_{T=T_c} = \frac{H_{c2}(T)}{T_c \times [-\frac{dH_{c2}(T)}{dT}]_{T=T_c}} = \frac{H_{c2}(T)}{H_{c2}(0)}$, of $Ag_{0.05}Bi_{1.95}Se_3$ at 11 and 20.5 GPa were plotted as a function of t $(=T/T_c)$ [Figs. 4(b) and 4(c)]. The $h^*(t)$–t plot shown in Fig. 4(b) reflects the low-T_c phase observed at 11 GPa since the T_c and H_{c2} are obtained from the R drop, as shown in Fig. 3(b). As seen from Fig. 4(b), the observed $h^*(t)$ value may not converge to 0.69 at $t = 0$, the value which is expected from the Werthamer-Helfand-Hohenberg theory, which refers to the s-wave dirty-limit superconductivity [25–27]. This behavior is the same as that of $Sr_{0.065}Bi_2Se_3$ [18]. The $h^*(0)$ value should become 0.80–0.85 for the p-wave polar model [18,26,28,29]. The observed $h^*(t)$–t plot [Fig. 4(b)] shows a linear relationship which may follow the p-wave model [see Fig. 4(b)]. However, the theoretical curve of s-wave clean limit may also follow the experimental h^*–t plot. As a consequence, the pressure-induced superconducting phase of $Ag_{0.05}Bi_{1.95}Se_3$ at 11 GPa may not definitely be identified to be an unconventional superconductor that follows the p-wave polar model, although the h^*–t plot of $Sr_{0.065}Bi_2Se_3$ at 19.5 GPa was followed by the above model [18]. Actually, the number of data points is insufficient for a complete identification of p-wave model for the pressure-induced superconducting phase of $Ag_{0.05}Bi_{1.95}Se_3$ at 11 GPa. In addition, the pressure-induced superconductivity of nondoped Bi_2Se_3 can also be classified as a topological superconductor from the $h^*(t)$–t plot [29]. Thus, we must obtain h^* values in a wider t range to finally determine whether the pressure-induced superconductivity in Ag-doped Bi_2Se_3 is explained by the p-wave polar model, in the same manner as Bi_2Se_3 [29] and Sr doped Bi_2Se_3 [18].

The $h^*(t)$–t plot for the high-T_c phase of $Ag_{0.05}Bi_{1.95}Se_3$ found at 20.5 GPa is shown in Fig. 4(c); the T_c and H_{c2} are obtained from the R drop due to the high-T_c phase shown in Fig. 3(d). As seen from Fig. 4(c), it is unclear whether the observed $h^*(t)$ values are followed by the p-wave model, because of insufficient h^* value against t. Thus, the pressure-induced superconducting phase (high-T_c phase: $T_c \sim 7$ K) of $Ag_{0.05}Bi_{1.95}Se_3$ at 20.5 GPa should also be more carefully investigated, in the same manner as the superconducting phase at 11 GPa [Fig. 4(b)].

IV. CONCLUSIONS AND OUTLOOK

Two pressure-driven superconducting phases were found in $Ag_{0.05}Bi_{1.95}Se_3$ at $p \geqslant 11$ GPa where two crystal phases (phase II and phase III) appeared. The low-T_c superconducting phase ($T_c = 5.5$ K) appeared at 11 GPa, and its T_c value decreased gradually with increasing pressure up to 15 GPa; the T_c value in the low-T_c phase became 3.6 K at 15 GPa and it did not vary up to 24 GPa. The high-T_c superconducting phase ($T_c = 7$ K) emerged suddenly at 17 GPa, and it did not change up to 26 GPa. The low-T_c and high-T_c phases coexisted up to 24 GPa. Above 24 GPa, only a high-T_c phase was observed. To sum up, the superconductivity in Ag-doped Bi_2Se_3 is superconductivity realized in hole-doped Bi_2Se_3, in which the Fermi level should be moved downward from the conduction band; the Fermi level of nondoped Bi_2Se_3 crosses the conduction band [9–11]. We could not definitely conclude whether the superconducting phases observed at 11 and 20.5 GPa can be categorized as unconventional topological superconductor which follows p-wave polar model, because of insufficient h^*–t plot. Nevertheless, this study may provide this research field with a useful starting point for studying topological superconductivity, as well as pressure-driven superconductivity. The mechanism of pressure-induced superconductivity in $Ag_xBi_{2-x}Se_3$ must be further pursued.

ACKNOWLEDGMENTS

This study was partly supported by Grants-in-Aid (Grants No. 26105004 and No. 17K05500) from MEXT, by JST ACT-C Grant No. JPMJCR12YW, Japan, and by the Program for Promoting the Enhancement of Research Universities. The XRD measurements at SPring-8 were carried out under Proposals No. 2017B4133 and No. 2017B4138, and the x-ray fluorescence holography at SPring-8 was measured under Proposals No. 2016A0124 and No. 2016B0124.

[1] C. L. Kane and E. J. Mele, Z_2 Topological Order and the Quantum Spin Hall Effect, Phys. Rev. Lett. **95**, 146802 (2005).

[2] J. E. Moore and L. Balents, Topological invariants of time-reversal-invariant band structures, Phys. Rev. B **75**, 121306(R) (2007).

[3] M. Z. Hasan and C. L. Kane, Colloquium: Topological insulators, Rev. Mod. Phys. **82**, 3045 (2010).

[4] D. Hsieh, D. Qian, L. Wray, Y. Xia, Y. S. Hor, R. J. Cava, and M. Z. Hasan, A topological Dirac insulator in a quantum spin Hall phase, Nature (London) **452**, 970 (2008).

[5] L. Fu and C. L. Kane, Topological insulators with inversion symmetry, Phys. Rev. B **76**, 045302 (2007).

[6] Y. Xia, D. Qian, D. Hsieh, L. Wray, A. Pal, H. Lin, A. Bansil, D. Grauer, Y. S. Hor, R. J. Cava, and M. Z. Hasan, Discovery (theoretical prediction and experimental observation) of a large-gap topological-insulator class with spin-polarized single-Dirac-cone on the surface, Nat. Phys. **5**, 398 (2009).

[7] Y. L. Chen, J. G. Analytis, J. H. Chu, Z. K. Liu, S. K. Mo, X. L. Qi, H. J. Zhang, D. H. Lu, X. Dai, Z. Fang, S.-C. Zhang, I. R. Fisher, Z. Hussain, and Z.-X. Shen, Experimental realization of a three-dimensional topological insulator, Bi_2Te_3, Science **325**, 178 (2009).

[8] D. Hsieh, Y. Xia, D. Qian, L. Wray, F. Meier, J. H. Dil, J. Osterwalder, L. Patthey, A. V. Fedorov, H. Lin, A. Bansil, D. Grauer, Y. S. Hor, R. J. Cava, and M. Z. Hasan, Observation of Time-Reversal-Protected Single-Dirac-Cone Topological-Insulator States in Bi_2Te_3 and Sb_2Te_3, Phys. Rev. Lett. **103**, 146401 (2009).

[9] N. P. Butch, K. Kirshenbaum, P. Syers, A. B. Sushkov, G. S. Jenkins, H. D. Drew, and J. Paglione, Strong surface scattering in ultrahigh-mobilityBi_2Se_3topological insulator crystals, Phys. Rev. B **81**, 241301(R) (2010).

[10] J. G. Analytis, J. H. Chu, Y. L. Chen, F. Corredor, R. D. McDonald, Z.-X. Shen, and I. R. Fisher, Bulk Fermi surface coexistence with Dirac surface state inBi_2Se_3: A comparison of photoemission and Shubnikov-de Haas measurements, Phys. Rev. B **81**, 205407 (2010).

[11] D. O. Scanlon, P. D. C. King, R. P. Singh, A. de la Torre, S. M. Walker, G. Balakrishnan, F. Baumberger, and C. R. A. Catlow, Controlling bulk conductivity in topological insulators: Key role of anti-site defects, Adv. Mater. **24**, 2154 (2012).

[12] Z. Y. Wang, T. Lin, P. Wei, X. F. Liu, R. Dumas, K. Liu, and J. Shi, Tuning carrier type and density in Bi_2Se_3 by Ca-doping, Appl. Phys. Lett. **97**, 042112 (2010).

[13] Y. S. Hor, A. Richardella, P. Roushan, Y. Xia, J. G. Checkelsky, A. Yazdani, M. Z. Hasan, N. P. Ong, and R. J. Cava, p-type Bi_2Se_3 for topological insulator and low-temperature thermoelectric applications, Phys. Rev. B **79**, 195208 (2009).

[14] Z. Ren, A. A. Taskin, S. Sasaki, K. Segawa, and Y. Ando, Optimizing $Bi_{2-x}Sb_xTe_{3-y}Se_y$ solid solutions to approach the intrinsic topological insulator regime, Phys. Rev. B **84**, 165311 (2011).

[15] T. Arakane, T. Sato, S. Souma, K. Kosaka, K. Nakayama, M. Komatsu, T. Takahashi, Z. Ren, K. Segawa, and Y. Ando, Tunable Dirac cone in the topological insulator $Bi_{2-x}Sb_xTe_{3-y}Se_y$, Nat. Commun. **3**, 636 (2012).

[16] Y. S. Hor, A. J. Williams, J. G. Checkelsky, P. Roushan, J. Seo, Q. Xu, H. W. Zandbergen, A. Yazdani, N. P. Ong, and R. J. Cava, Superconductivity in $Cu_xBi_2Se_3$ and its Implications for Pairing in the Undoped Topological Insulator, Phys. Rev. Lett. **104**, 057001 (2010).

[17] Z. H. Liu, X. Yang, J. F. Shao, M. Zuo, L. Pi, S. Tan, C. J. Zhang, and Y. H. Zhang, Superconductivity with topological surface state in $Sr_xBi_2Se_3$, J. Am. Chem. Soc. **137**, 10512 (2015).

[18] Y. H. Zhou, X. L. Chen, R. R. Zhang, J. F. Shao, X. F. Wang, C. An, Y. Zhou, C. Y. Park, W. Tong, L. Pi, Z. R. Yang, C. J. Zhang, and Y. H. Zhang, Pressure-induced reemergence of superconductivity in topological insulator $Sr_{0.065}Bi_2Se_3$, Phys. Rev. B **93**, 144514 (2016).

[19] P. P. Kong, J. L. Zhang, S. J. Zhang, J. Zhu, Q. Q. Liu, R. C. Yu, Z. Fang, C. Q. Jin, W. G. Yang, X. H. Yu, J. L. Zhu, and Y. S. Zhao, Superconductivity of the topological insulator Bi_2Se_3 at high pressure, J. Phys.: Condens. Matter **25**, 362204 (2013).

[20] T. Asaba, B. J. Lawson, C. Tinsman, L. Chen, P. Corbae, G. Li, Y. Qiu, Y. S. Hor, L. Fu, and L. Li, Rotational Symmetry Breaking in a Trigonal Superconductor Nb-Doped Bi_2Se_3, Phys. Rev. X **7**, 011009 (2017).

[21] M. I. Zargarova, P. K. Babaeva, D. S. Azhdarova, Z. D. Melikova, and S. A. Mekhtieva, A study of the systems $CuInSe_2$-InSe ($SnSe_2$,Bi_2Se_3), Inorg. Mater. **31**, 263 (1995).

[22] E. Uesugi, T. Uchiyama, H. Goto, H. Ota, T. Ueno, H. Fujiwara, K. Terashima, T. Yokoya, J. Akimitsu, K. Kobaysashi, and Y. Kubozono (unpublished).

[23] K. Hayashi, N. Happo, S. Hosokawa, W. Hu, and T. Matsushita, X-ray fluorescence holography, J. Phys.: Condens. Matter **24**, 093201 (2012).

[24] J. J. Barton, Removing Multiple Scattering and Twin Images from Holographic Images, Phys. Rev. Lett. **67**, 3106 (1991).

[25] N. R. Werthamer, E. Helfand, and P. C. Hohenberg, Temperature and purity dependence of the superconducting critical field, H_{c2}. III. Electron spin and spin-orbit effects, Phys. Rev. **147**, 295 (1966).

[26] K. Scharnberg and R. A. Klemm, P-wave superconductors in magnetic fields, Phys. Rev. B **22**, 5233 (1980).

[27] E. Helfand and N. R. Werthamer, Temperature and purity dependence of the superconductivity critical field, H_{c2}. II, Phys. Rev. **147**, 288 (1966).

[28] K. Maki, E. Puchkaryov, G.-F. Wang, and H. Won, Aspects of p-wave superconductivity, Chin. J. Phys. **38**, 386 (2000).

[29] K. Kirshenbaum, P. S. Syers, A. P. Hope, N. P. Butch, J. R. Jeffries, S. T. Weir, J. J. Hamlin, M. B. Maple, Y. K. Vohra, and J. Paglione, Pressure-Induced Unconventional Superconducting Phase in the Topological Insulator Bi_2Se_3, Phys. Rev. Lett. **111**, 087001 (2013).